J Nanopart Res (2013) 15:1662
DOI 10.1007/s11051-013-1662-x

RESEARCH PAPER

Red shift in absorption edge of $Cd_{1-x}Ni_xS$ dilute magnetic semiconductor nanofilms

Suresh Kumar · Pankaj Sharma · Vineet Sharma

Received: 8 January 2013 / Accepted: 15 April 2013 / Published online: 26 April 2013

Abstract Nickel-doped cadmium sulphide dilute semiconductor nanofilms ($Cd_{1-x}Ni_xS$, $0 \leq x \leq 0.09$) have been investigated using atomic force microscopy, scanning electron microscopy, Fourier infrared transform and UV–Vis spectroscopy. With increasing Ni content a decrease in average crystallite size (26–10 nm) and surface roughness has been found. A red shift in optical band gap has been observed with decrease in average crystallite size, which is against quantum confinement.

Keywords Dilute magnetic semiconductors · Optical band gap · Morphology

Introduction

In the present research scenario of devising multifunctional materials, dilute magnetic semiconductors (DMS) have acquired an indispensable place in the field of spintronics, non-volatile memories, quantum computing, communication in the solid state, magneto-optical devices etc. (Dietl et al. 2000; Dietl 2008; Ohno 2010; Radovanovic et al. 2005; Chelikowsky et al. 2006; Jungwirth et al. 2006). DMS are produced by replacing some of the cations in the host semiconductor (especially group II–VI and III–V) with magnetic ions particularly transition metal (TM) like Fe, Mn, Ni, Co etc. (Furdyna 1988; Malguth et al. 2008; Wu et al. 2006; Schwartz et al. 2004; Ozer et al. 2012). The spin-exchange (*sp–d*) interaction between the semiconductor charge carriers and magnetic ions add local magnetic moments in DMS and accumulate magneto-opto-electronic character in them. The introduction of dopant in II–VI semiconductors is an extensive route to tune them with respect to the phase, morphology and crystallite size. TM-doped CdS films provide an opportunity to integrate various properties into a single material for advanced applications (Chelikowsky et al. 2006; Wu et al. 2006; Saravanan et al. 2011; Kamruzzaman et al. 2012; Polat et al. 2012; Chandramohan et al. 2009; Kim et al. 1993).

In this communication, we report the investigation of $Cd_{1-x}Ni_xS$ ($0 \leq x \leq 0.09$) DMS nanofilms via FTIR, SEM, AFM and UV–Vis spectroscopy. We observed and studied for the structure, surface morphology and optical band gap.

Experimental

A detailed experimental procedure for deposition of $Cd_{1-x}Ni_xS$ ($0 \leq x \leq 0.09$) DMS nanofilms is given elsewhere (Kumar et al. 2013; Kumar et al. 2012a,

S. Kumar · P. Sharma (✉) · V. Sharma
Department of Physics and Materials Science, Jaypee University of Information Technology, Waknaghat, Solan 173234, HP, India
e-mail: pks_phy@yahoo.co.in

2012b). The thickness of nanofilms (Table 1) was measured by stylus profilometer (AMBIOS XP-1). Surface morphology was studied using field emission scanning electron microscope (FE-SEM, HITACHI S-4700) and AFM (NTMDT-NTEGRA) in semi-contact mode. FTIR (Perkin Elmer 1600 FTIR spectrophotometer) measurements were obtained in the spectral range 400–4000 cm^{-1}. UV–Vis–NIR double beam spectrophotometer (Perkin Elmer, Lambda-750) was used to obtained transmittance (*%T*) and reflectance (*%R*) spectra in the wavelength range 300–900 nm.

Results and discussion

The structural analysis of $Cd_{1-x}Ni_xS$ DMS nanofilms has been performed using XRD and given elsewhere (Kumar et al. 2013). All the nanofilms have prominent reflection peaks associated with α-CdS structure in conjunction with other low-intensity reflection peaks assigned either α-CdS or both α and β-CdS (Kumar et al. 2013).

FTIR spectra for $Cd_{1-x}Ni_xS$ nanofilms (Fig. 1) show various absorption bands/peaks at different frequencies. The absorption bands/peaks at ~3400–3430 cm^{-1}, 1438–1450 cm^{-1}, 860–900 cm^{-1}, 1370–1400 cm^{-1} and 1990–2150 cm^{-1} and weak doublet at 2920 and 2851 cm^{-1} have been assigned for O–H stretching, asymmetric scissor deformation (δ_{as}-CH_2), hydrogen bound O–H out of plane bending, primary or secondary OH in-plane bending, isothiocyanate (–NCS) formed due to thiourea dissociation, asymmetrical and symmetrical vibration of CH_2 group (υ_{as}-CH_2 and υ_s-CH_2), respectively (Coates 2000; Thangadurai et al. 2008; Cabana et al. 2011). The peak at ~1011 cm^{-1} ($x = 0$) and ~1075 cm^{-1} ($x = 0.02$–0.09) belongs to primary amine C–N stretch (Coates 2000) and also shared by C–O stretching (Thangadurai et al. 2008). However, secondary amine C–N stretch is indicated by peaks at 1399 cm^{-1} ($x = 0$) and ~1370 cm^{-1} ($x = 0.02$–0.09) (Coates 2000). These peaks of

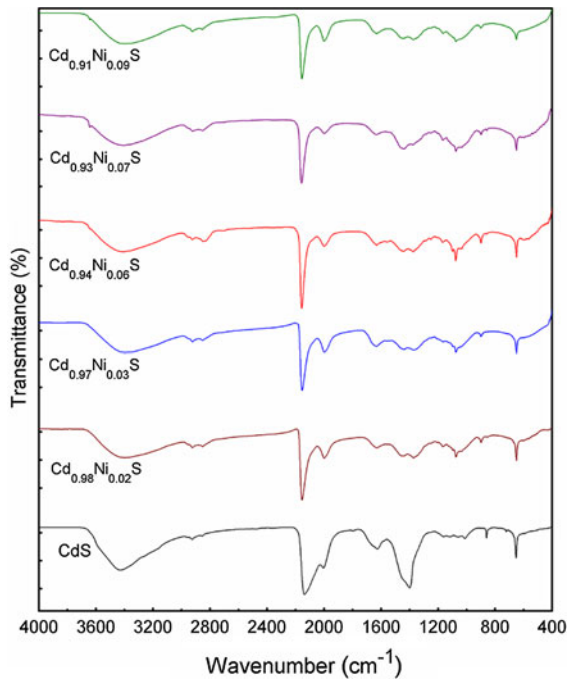

Fig. 1 FTIR spectra for $Cd_{1-x}Ni_xS$ ($0 \le x \le 0.09$) nanofilms (The ordinate scale for different x values is shifted for clarity)

Table 1 The compositional, morphological and optical parameters of $Cd_{1-x}Ni_xS$ ($0 \le x \le 0.09$) nanofilms, where $x_m = \left(\frac{Ni}{Cd + Ni}\right)_{Solution}$ is the solution concentration from molarities and $x_f = \left(\frac{Ni}{Cd + Ni}\right)_{Film}$ is the film composition from EDAX

Sample	x_m	x_f	Film thickness (nm)	AFM		α ($\times 10^4$ cm^{-1})	E_u (eV)
				D_{AFM} (nm)	R_f (nm)		
CdS	0	0	67.6	26	9.6	1.01	0.282
$Cd_{0.98}$ $Ni_{0.02}S$	0.05	0.02	79.4	21	5.2	2.65	0.291
$Cd_{0.97}$ $Ni_{0.03}S$	0.09	0.03	83.5	17	5.1	2.73	0.332
$Cd_{0.94}$ $Ni_{0.06}S$	0.13	0.06	88.4	15	5.0	2.77	0.372
$Cd_{0.93}$ $Ni_{0.07}S$	0.17	0.07	92.2	15	3.1	5.32	0.490
$Cd_{0.91}$ $Ni_{0.09}S$	0.20	0.09	103.8	10	4.5	6.80	0.509

C–N stretching are evolved due to alkaline nature of solution because of the presence of TEA and NH_3. $Cd_{1-x}Ni_xS$ ($x \geq 0.03$) nanofilms have small peaks in the region 470–600 cm^{-1} belonging to S–S stretch (Coates 2000). All nanofilms have a strong absorption peak at $\sim$650 cm^{-1} associated with Cd–S stretching (Thangadurai et al. 2008). No peak for Ni–S stretching has been observed which indicates homogeneous substitution of Ni^{2+} ions in CdS structure. The shift of Cd–S stretch ($\sim$650 cm^{-1}) towards lower wavenumber with increasing x indicates the incorporation of Ni^{2+} ions in the CdS structure.

Figure 2 shows micro-structural surface morphology for $Cd_{1-x}Ni_xS$ nanofilms at a scale of 1 μm (50 K×). All nanofilms show uniformly distributed spherical nanocrystallites on the surface of substrate

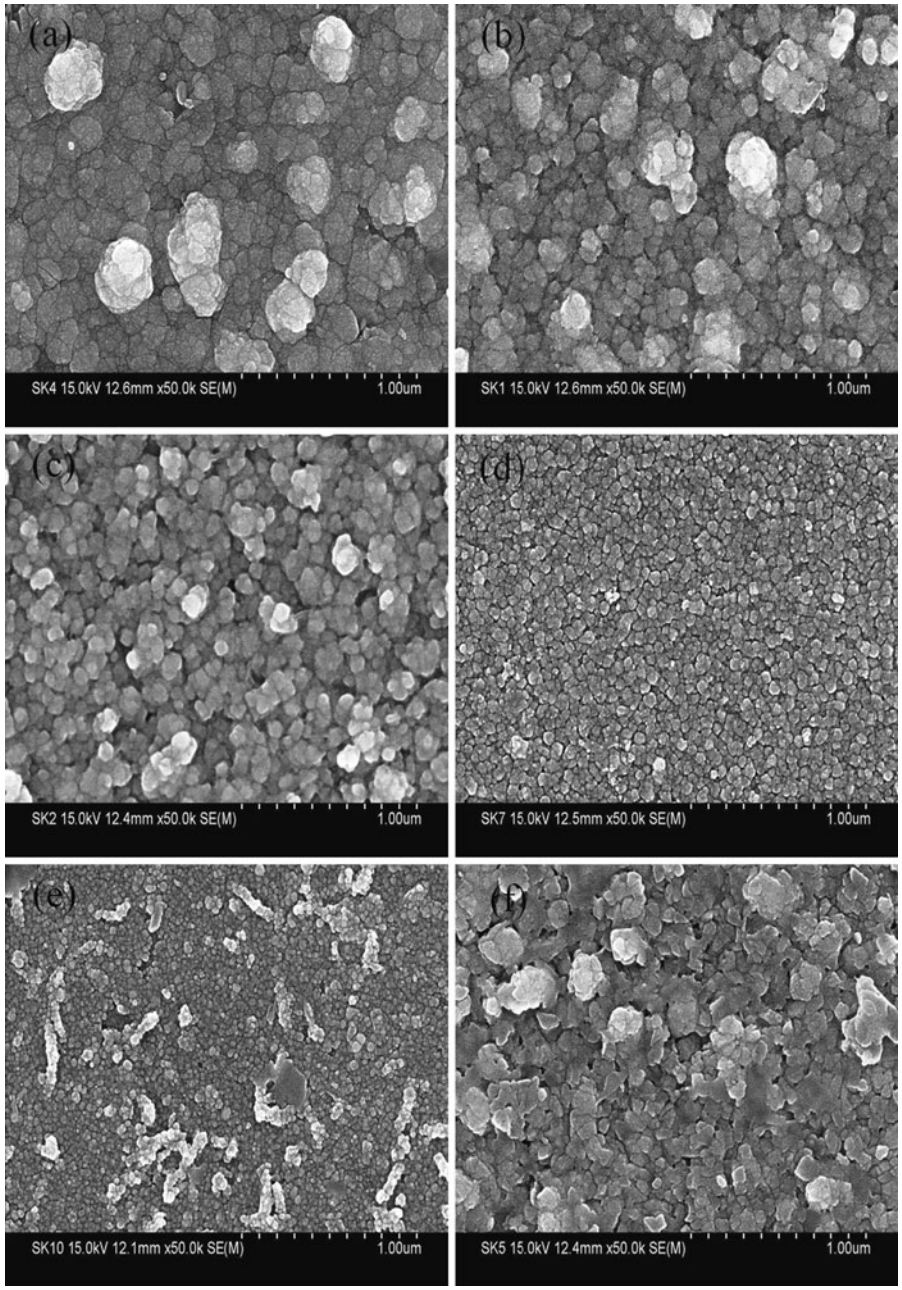

Fig. 2 SEM micrographs for $Cd_{1-x}Ni_xS$ nanofilms (**a** $x = 0$, **b** $x = 0.02$, **c** $x = 0.03$, **d** $x = 0.06$, **e** $x = 0.07$ and **f** $x = 0.09$)

with good adhesion. The surface of all films is compact, densely packed, continuous and barren free which may be attributed to chemical activity of triton (TX-100) (Kumar et al. 2012a). Surface morphology of nanofilms is strongly dependent on Ni content. The substitution of Ni^{2+} ions in CdS structure produces substantial surface changes with less agglomeration of the crystallites i.e. reduction in crystallite size and increase in grain boundaries. The nanofilm $x = 0.07$ shows sphere-like crystallite chains in an irregular spatial distribution. However, surface morphology for $x = 0.09$ is quite different, showing sheet-like structural growth.

The surface topography and structure of film surfaces are shown in Fig. 3 (AFM-2D images) and Fig. 4 (AFM-3D images) of DMS nanofilms. Nanofilm with $x = 0$ (Fig. 3a) possesses larger crystallites (D_{AFM}) and high average surface roughness (R_f) (Table 1). However, with increasing Ni^{2+} concentration (Fig. 3a–f) the D_{AFM} of $Cd_{1-x}Ni_xS$ nanofilms decreases. R_f also decreases up to $x \leq 0.07$. The low value of surface skewness ($S_{sk} < 0.7$) and kurtosis

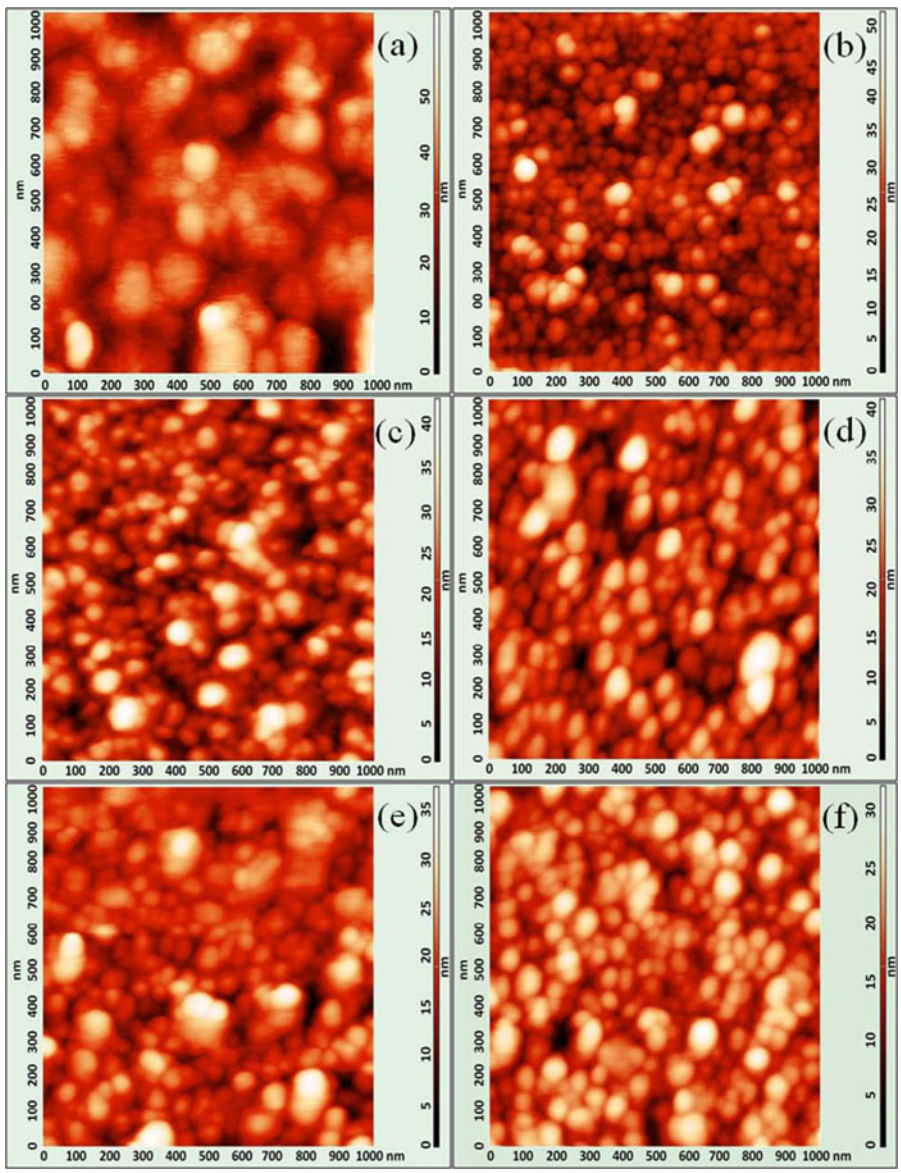

Fig. 3 AFM-2D images for $Cd_{1-x}Ni_xS$ nanofilms (**a** $x = 0$, **b** $x = 0.02$, **c** $x = 0.03$, **d** $x = 0.06$, **e** $x = 0.07$ and **f** $x = 0.09$)

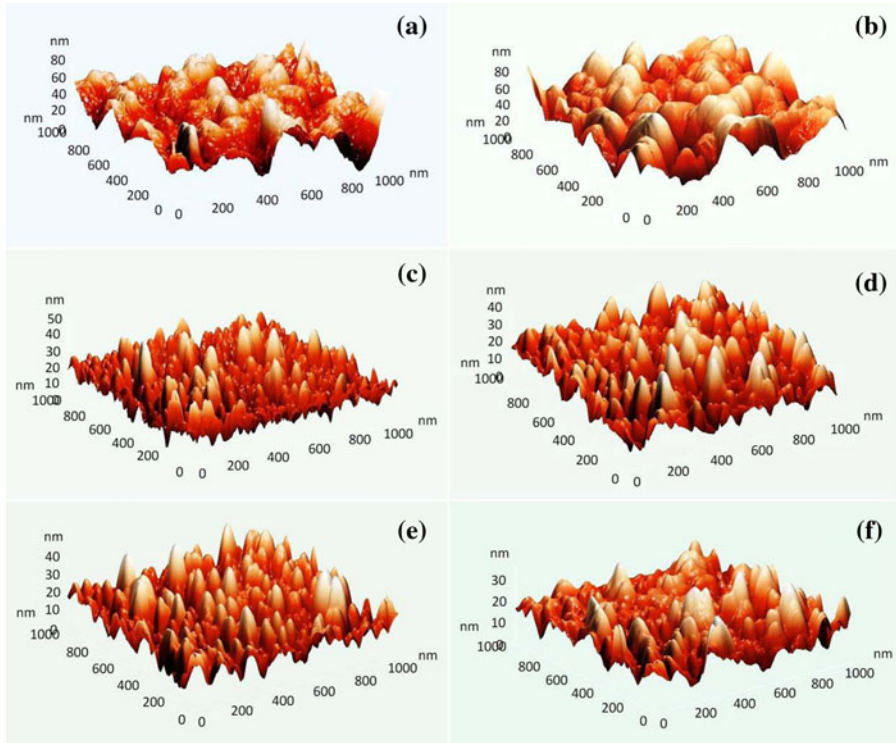

Fig. 4 AFM-3D images for $Cd_{1-x}Ni_xS$ nanofilms (**a** $x = 0$, **b** $x = 0.02$, **c** $x = 0.03$, **d** $x = 0.06$, **e** $x = 0.07$ and **f** $x = 0.09$)

coefficient ($S_{ka} \geq 3$) for all nanofilms indicate that the height distribution is uniform, with approximately equal number of high peaks to deep valleys (Fig. 4a–f) over the scanned area (1 μm × 1 μm). All films grow with columnar structures along the c-axis perpendicular to the substrate which confirm the prominent hexagonal-wurtzite structure in deposited $Cd_{1-x}Ni_xS$ nanofilms (Lazos et al. 2008).

Figure 5 shows $\%T$ and $\%R$ spectra of DMS nanofilms grown on glass substrate. The occurrence of low $\%T$ interference pattern in spectra indicates that the deposited nanofilms are ultra thin, smooth and homogeneous. High $\%T$ (>65 %) and low $\%R$ (<20 %) in the visible region makes these films good candidate for solar energy applications.

The optical behaviour of deposited DMS nanofilms have been analyzed in term of optical absorption coefficient (α) (Salem et al. 2008). The value of α for all nanofilms has been found to be $\sim 10^5$ cm^{-1} in the visible region, and at absorption edge, α increases with increasing x (Table 1). This may be due to decrease in crystallite size which provides large collective surface area and large number of absorption/scattering centres for light. The exponential dependence of α on photon energy (hv) near the band edge has been studied in terms of Urbach energy (E_u) by Urbach–Martienssen model (Pejova 2010). E_u is often interpreted as the width of the tail of localized states in the gap region (for the values of E_u see Table 1). A systematic increase in E_u may be attributed to the creation of more localized states within the band tails of valence and conduction band due to the existence of defects and disorders. A sharp fall in $\%T$ (Fig. 5) near the fundamental absorption edge indicates a direct energy transition in the forbidden gap. The optical band gap (E_g) for direct transition has been determined using Tauc's relation (Kumar et al. 2012b). The E_g values have been estimated by extrapolating $(\alpha hv)^2 \rightarrow 0$ (Fig. 6). The band gap decreases with increasing Ni content in CdS nanofilms (Fig. 7).

The variation of $E_g(x_f)$ with film composition (x_f) (inset Fig. 7) indicates non-linear behaviour showing bowing phenomenon following Vegard's law (Li et al. 2011). The red shift in band edge on Ni doping (Fig. 6) indicates narrowing of band gap even with decrease in crystallite size. This may be attributed to structural disorders, increased tail width of localized states (E_u) (Table 1) and *sp–d* hybridization effect. Ni^{2+} ions in the host CdS crystal form new localized electronic states in the band gap, which arise from the 3*d*-shell of

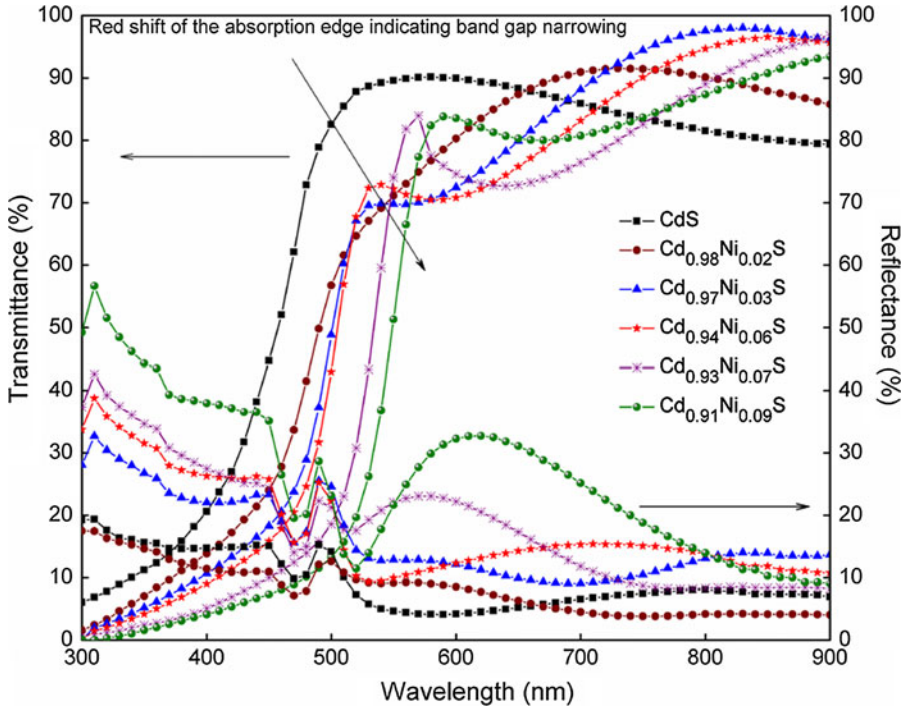

Fig. 5 *%T* and *%R* spectra for $Cd_{1-x}Ni_xS$ nanofilms ($0 \leq x \leq 0.09$)

Ni^{2+} ion under the action of surrounding CdS crystal field (Podlowski et al. 1992). With an increase in Ni^{2+} ion concentration, the *sp–d* exchange interaction between the band electrons and the localized *d*-electrons of Ni^{2+} ions increases (Polat et al. 2012; Kim et al. 1993). The strength of this interaction strongly depends on the number of *d*-electrons (Samanta et al. 2009). The reduction of crystallite

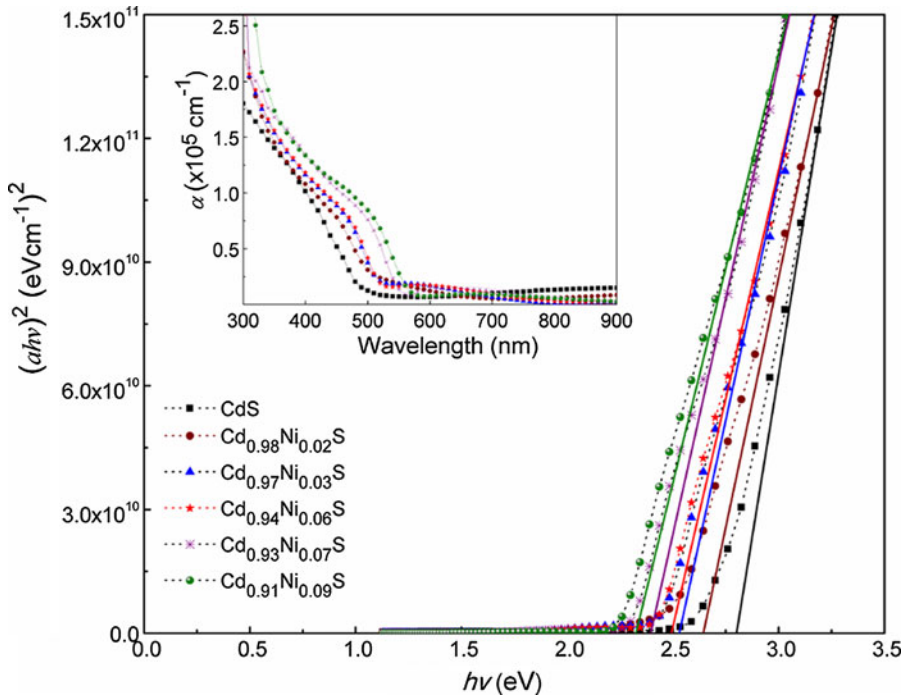

Fig. 6 Tauc's plot for $Cd_{1-x}Ni_xS$ ($0 \leq x \leq 0.09$) nanofilms and inset show α *vs.* wavelength

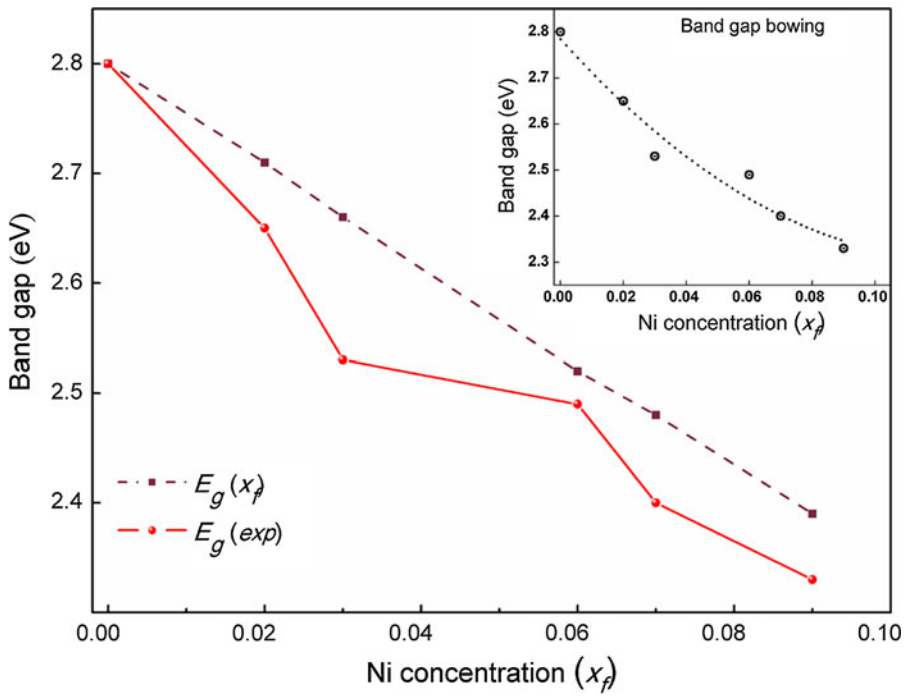

Fig. 7 Variation of E_g with Ni concentration (x_f) and inset show band gap bowing

size with doping of Ni^{2+} ions also leads to an increase in surface/volume ratio. As a result, the surface states corresponding to Ni^{2+} in CdS increase and reduce the excitonic emission via non-radiative surface recombination (Podlowski et al. 1992). The Ni doping creates high density of impurity states in the nanofilms, which may also perturbate the band structure in the energy gap. The impurity band merges with the nearest intrinsic band and the Fermi level may lie inside the parabolic portion of the valence band (Oztas et al. 2007). Thus, less energy will be required for the electrons to move from the Fermi level into the conduction band (Oztas et al. 2007). The dopant ions form deep trap levels, which act as luminescence centres, create more discrete energy states by modifying the band structure.

Conclusion

The morphology and optical behaviour of II–VI DMS have been reported. Ni^{2+} ions in CdS show change in absorption peak position ($\sim$650 cm^{-1}) and the strength of respective vibrational bands indicate the incorporation of Ni in host CdS lattice. The surface morphology depends on Ni^{2+} concentration and shows less agglomeration of the crystallites with increase in grain boundaries and decrease in surface roughness on an increase in Ni content. The red shift in band edge on incorporation of Ni^{2+} ions in CdS show band gap narrowing with decrease in crystallite size. This may be attributed to creation of localized states within the band tails and *sp–d* hybridization effect. The high transmittance and band gap tailoring of DMS nanofilms from 2.80 to 2.33 eV in visible region and UV end of solar spectrum make them suitable for large area coating of photovoltaic devices, anti-reflection coating, solar control coating and warming window layers.

Acknowledgments The authors acknowledge PU Chandigarh, IIT-Roorkee and JUIT Solan for providing FTIR, SEM & AFM and UV–Vis–NIR facility, respectively.

References

Cabana ZL, Torres CMS, Gonzalez G (2011) Semiconducting properties of layered cadmium sulphide-based hybrid nanocomposites. Nanoscale Res Lett 6:523 (8)

Chandramohan S, Kanjilal A, Tripathi JK, Sarangi SN, Sathyamoorthy R, Som T (2009) Structural and optical properties of Mn-doped CdS thin films prepared by ion implantation. J Appl Phys 105:123507/1–123507/4

Chelikowsky JR, Kaxiras E, Wentzcovitch RM (2006) Theory of spintronic materials. Phys Stat Sol (b) 243:2133–2150

Coates J (2000) Interpretation of IR spectra: a practical approach. In: Mayers RA (ed) Encyclopedia of analytical chemistry. Wiley, Chichester, pp 10815–10837

Dietl T (2008) Hole states in wide band-gap diluted magnetic semiconductors and oxides. Phys Rev B 77:085208/1–085208/6

Dietl T, Ohno H, Matsukura F, Cibet J, Ferrand D (2000) Zener model description of ferromagnetism in zinc-blende magnetic semiconductors. Science 287:1019–1022

Furdyna JK (1988) Diluted magnetic semiconductors. J Appl Phys 64:R29–R64

Jungwirth T, Sinova J, Masek J, Kucera J, MacDonald AH (2006) Theory of ferromagnetic (III,Mn)V semiconductors. Rev Mod Phys 78:809–864

Kamruzzaman M, Luna TR, Podder J, Anowar MGM (2012) Synthesis and characterization of $Cd_{1-x}Co_xS$ thin films prepared using the spray pyrolysis technique. Semicond Sci Technol 27:035017/1–035017/6

Kim YD, Chang YC, Klein MV (1993) Effect of *d* electrons in transition-metal ions on band-gap energies of diluted magnetic semiconductors. Phys. Rev. B 48:17770–17775

Kumar S, Sharma P, Sharma V (2012a) CdS nanofilms: synthesis and the role of annealing on structural and optical properties. J Appl Phys 111:043519/1–043519/6

Kumar S, Sharma P, Sharma V (2012b) Structural transition in II–VI nanofilms: effect of molar ratio on structural, morphological, and optical properties. J Appl Phys 111:113510/1–113510/6

Kumar S, Sharma P, Sharma V (2013) Phase transition in II–VI nanofilms of dilute magnetic semiconductors: $Cd_{1-x}Ni_xS$. Sci Adv Mater 5. doi:10.1166/sam.2013.1505

Lazos CDG, Rosendo E, Juarez BH, Salgado GG, Diaz T, Falfan MR, Oliva AI, Quintana P, Aguilar DH, Cauich W, Ortega M, Matsumoto Y (2008) Hexagonal phase of CdS thin Films obtained by oscillating chemical bath. J Electrochem Soc 155:D158–D162

Li L, Muckerman JT, Hybertsen MS, Allen PB (2011) Phase diagram, structure, and electronic properties of $(Ga_{1-x}Zn_x)(N_{1-x}O_x)$ solid solutions from DFT-based simulations. Phys Rev B 83:134202/1–134202/6

Malguth E, Hoffmann A, Phillips MR (2008) Fe in III–V and II–VI semiconductors. Phys Stat Sol (b) 245:455–480

Ohno H (2010) A window on the future of spintronics. Nature Mater 9:952–954

Ozer MM, Thompson JR, Weitering HH (2012) Growth and magnetic properties of Mn doped germanium near the kinetic solubility limit. Phys Rev B 85:125208/1–125208/7

Oztas M, Bedir M, Ocak S, Yildirim RG (2007) The role of growth parameters on structural, morphology and optical properties of sprayed ZnS thin films. J Mater Sci Mater Electron 18:505–512

Pejova B (2010) The Urbach-Martienssen absorption tails in the optical spectra of semiconducting variable-sized zinc selenide and cadmium selenide quantum dots in thin film form. Mater Chem Phys 119:367–376

Podlowski L, Heitz R, Hoffman A, Broser I (1992) Nonradiative recombination processes of Ni-impurities in CdS and ZnS. J Lumin 53:401–405

Polat I, Aksu S, Altunbas M, Bacaksz E (2012) The influence of diffusion temperature on the structural, optical and magnetic properties of nickel-doped zinc oxysulfide thin films. Phys Status Solidi A 209:160–166

Radovanovic PV, Barrelet CJ, Gradecak S, Qian F, Lieber CM (2005) General synthesis of manganese-doped II–VI and III–V semiconductor nanowires. Nano Lett 5:1407–14011

Salem AM, El–Gendy YA, Sakr GB, Soliman WZ (2008) Optical properties of thermochromic Cu_2HgI_4 thin films. J Phys D 41:025311/1–025311/7

Samanta K, Bhattacharya P, Katiyar RS (2009) Microstructural and ferromagnetic properties of $Zn_{1-x}Cu_xO$ thin films. J Appl Phys 105:113929/1–113929/4

Saravanan L, Pandurangan A, Jayavel R (2011) Synthesis of cobalt-doped cadmium sulphide nanocrystals and their optical and magnetic properties. J Nanopart Res 13:1621–1628

Schwartz DA, Kittilstved KR, Gamelin DR (2004) Above-room-temperature ferromagnetic Ni^{2+}-doped ZnO thin films prepared from colloidal diluted magnetic semiconductor quantum dots. Appl Phys Lett 85:1395–1397

Thangadurai P, Balaji S, Manoharan PT (2008) Surface modification of CdS quantum dots using thiols-structural and photophysical studies. Nanotechnology 19:435708(8 pp)

Wu XJ, Shen DZ, Zhang ZZ, Zhang JY, Liu KW, Li BH, Lu YM, Zhao DX, Yao B (2006) *p*-type conductivity and donor-acceptor pair emission in $Cd_{1-x}Fe_xS$ dilute magnetic semiconductors. Appl Phys Lett 89:262118/1–262118/3